

Original scientific paper

NUMERICAL SIMULATION OF DYNAMICS OF BLOCK MEDIA BY MOVABLE LATTICE AND MOVABLE AUTOMATA METHODS

Alexander E. Filippov^{1,2}, Valentin L. Popov²

¹Donetsk Institute for Physics and Engineering, Donetsk, Ukraine

²Technische Universität Berlin, Berlin, Germany

Abstract. *Two versions of modified Burridge-Knopoff model including state dependent friction, elastic force and thermal conductivity are derived. The friction model describes a velocity weakening of friction and elasticity between moving blocks and an increase of both static friction and rigidity during stick periods as well their weakening during motion. It provides a simplified but qualitatively correct behavior including the transition from smooth sliding to stick-slip behavior, which is often observed in various tribological and tectonic systems. Attractor properties of the model dynamics is studied also. The alternative versions of the model are proposed which apply a simulation of the motion of interacting elastically connected mesh elements and motion of relatively large solid blocks, utilizing technique of the movable cellular automata. First version of the model was already basically studied before. Its advanced version here involves all components of the real system: state-dependending friction and changeable rigidity, as well as heat production and thermal conductivity. Model based on the movable automata also involves the components included into traditional lattice model. It has its own ad-vantages and disadvantages which are also discussed in the paper.*

Key words: *Burridge-Knopoff model, Friction, Tectonics, Voronoi diagram, Delaunay triangulation*

1. INTRODUCTION

One of the most important applications in the study of the behavioral patterns of mechanical systems of block structures are the geological faults and block environments. Of particular interest, of course, is the study of the possible variations of their deformation, potential prediction or even prevention of the strong seismic shocks. The fact that the statistics of earthquake force and their time correlations meet the laws of Gutenberg-Richter [1,2] and Omori [1,3], typical for self-organized critical systems [4,5],

Received: March 27, 2022 / Accepted April 23, 2022

Corresponding author: Alexander E. Filippov

Donetsk Institute for Physics and Engineering, R. Luxemburg Str. 72, 83114 Donetsk, Ukraine

E-mail: filippov_ae@yahoo.com

is often the basis for the conclusion that earthquakes are a process formed on all spatial scales ranging from microscopic to continental plate scale. During last decades [6,10] on the basis of modeling by movable cellular automata and full-scale experiments it was shown some possibility of initiation of the fault wing displacement and, consequently, the release of a part of the accumulated elastic energy as a result of local effects on the fault area, including vibration load and watering [11-16].

One of the often applied to study the problems under interest is the well-known Burridge-Knopoff (BK) model [17,18] initially proposed many years ago to investigate statistical properties of earthquakes. Numerical studies by Carlson et al. [19,20] have demonstrated that BK model can reproduce characteristic empirical features of tectonic processes such as the Gutenberg-Richter law for the magnitude distribution of earthquakes, or the Omori law for statistics of aftershocks [19-22], both properties stemming from the so called “self-organized criticality” of this system. It has been intensively used to simulate different aspects of the problem [21-40] and to discuss general properties of earthquakes statistics as well as predictability of earthquakes. Numerical simulations give evidences that the self-organized criticality and the corresponding fractal attractor of the system is closely related to dynamic structures with “traveling waves” [23], their ordering and specific “phase transitions” [24] controlled by a number of parameters (external driving velocity, springs stiffness, number of blocks, their mutual interaction and so on). It is in particular the dependence of the dynamic properties of the BK model on spring stiffness which makes it necessary to introduce the generalization of the friction law proposed in the works [41,17].

The physical reason for the stick-slip instability in the Burridge-Knopoff model is the assumed decrease of the friction force with the sliding velocity [19,20]. Motion of a single block with this friction law is always unstable which does not correspond to properties of real tribological systems. The real law of rock friction is more complicated [29,34]. In this article we base on the realistic friction laws described in the handbooks [34,35]. The main qualitative pictures of a realistic law are: (a) approximately logarithmic increase of the static friction force as a function of contact time – the property, found already by Coulomb, and (b) a logarithmic dependence of the sliding friction on the sliding velocity. Both properties can be described in the frame of “state dependent” friction laws by introducing additional internal variables describing the state of the contact [17,41-43] as well as shear band propagation effect on the deformation and fracture [44,45], generation and propagation of slow deformation in geomedia [46-48].

Modified version of the BK model with a state dependent friction force, reproduces in the simplest way both the velocity weakening friction and the increase of static friction with time when the block is not moving.

2. METHOD

Let us briefly remind the original BK model. The blocks of mass m are attached to a moving surface by springs with stiffness k_1 and are coupled to each other by springs with stiffness k_2 . The moving surface has velocity v , and the blocks are in contact with a rough substrate. The friction force F between the blocks and the rough surface is assumed to depend only on velocity. The equations of the BK model can be written in the following form:

$$m \frac{\partial^2 u_j}{\partial t^2} = k_2 (u_{j+1} + u_{j-1} - 2u_j) + k_1 (vt - u_j) - F(v_j), \quad (1)$$

where $v = \text{const}$ is the external driving velocity and $v_j = \partial u_j / \partial t$ is an array of individual block velocities ($j=1, \dots, N$). The sliding friction force is supposed to decrease monotonously from a constant initial value F_0 . It is further supposed that the static friction $F(v_j \rightarrow 0)$ can possess any necessary negative value to prevent back sliding

$$F(v_j) = \begin{cases} \frac{F_0}{1 + 2\alpha v_j / (1 - \sigma)}, & F_0 = 1 - \sigma; \quad \partial u_j / \partial t > 0 \\ (-\infty, 0] & \partial u_j / \partial t = 0 \end{cases} \quad (2)$$

The parameter α defines a rate of friction decrease when block starts to slide, and σ is the acceleration of a block at instant when slipping begins [19,20]. The friction equation (2) is an oversimplification of real properties of static and kinetic friction which is now explained in detail in the books [34,35]. Dieterich has proposed friction equations with internal variables [29,30], where the friction force is dependent upon an additional variable that describes the state of the contact zone. This variable is in a sense a “melting parameter.” Friction force at non-zero velocity drops down from its initial value due to a “shear melting” effect which may have different physical nature [17-20]. When the motion stops, the surfaces start to form new bonds and the static friction increases with time.

The dynamics of systems with state dependent friction has been investigated in a number of papers [29-37]. Majority of these studies were devoted to the simple one-particle version of the model, but it was also done for many-body BK model with a state dependent friction [17], where the friction force is defined by the additional kinetic equation:

$$\frac{\partial F_j[v_j(t)]}{\partial t} = \beta_1 (F_0 - F_j) + \beta_2 v_j \quad (3)$$

with $\beta_2 < 0$, at $v_j > 0$, and $F(v_j) = -\infty$ in opposite case $v_j \leq 0$. The parameters β_1 and β_2 have following meaning. When a block starts to slide with $v_j > 0$ its friction force monotonously decreases from an initial value F_0 . General time scale of this process is determined by the first parameter β_1 and an effectiveness of the melting is given by a relation between absolute value of negative parameter $\beta_2 < 0$ and β_1 . It should be noted that the kinetic equations for state dependent friction at sliding are not unique. Different forms of this equation have been proposed [17,18] leading to qualitatively similar behavior of the dynamic friction at $v_j > 0$. The above form is just simplest and even linear one.

The equations of motion in Eqs. (1-3) are nonlinear wave equations. Last few decades different variants of such equations have been widely studied, starting from the very early implementation of the numerical simulations [38]. In particular, it has been shown that N interacting segments of the nonlinear chain form a collective attractor with energy transfer performed by nonlinear excitations [39,40]. Depending on the relations between total energy and strength of the interaction between the blocks k_2 , the chain can form nearly uniform or strongly non-uniform structures and phase patterns.

Analogous behavior should be expected in the modified Burridge-Knopoff model as well. Instantaneously moving blocks must be involved with stationary ones in the overall motion. This causes a “detachment” wave, propagating along the chain. Such waves were found and studied in the original BK model [18], and the analogous process exists in the modified one. There are two possible types of traveling waves: (a) after a transition time all the blocks are provoked to move simultaneously, (b) in steady state some of the blocks can be found instantaneously motionless while others move. One would expect the reaction of the chain to depend on the strength of the interaction between the blocks. This question has been studied for the original BK model in [20], and a specific “phase transition” between correlated and uncorrelated behavior has been found.

Real contact of two surfaces is two-dimensional. Let us generalize the MBK to the case. The generalized model is very similar to the one-dimensional model but incorporates a 2D array of blocks connected by elastic springs in both directions. All other components of the MBK remain unchanged.

The system of equations of motion takes the form:

$$m \frac{\partial^2 u_{j,n}}{\partial t^2} = k_2 (u_{j+1,n} + u_{j-1,n} + u_{j,n+1} + u_{j,n-1} - 4u_{j,n}) - \eta \frac{\partial u_{j,n}}{\partial t} + k_1 (vt - u_{j,n}) + F(v_{j,n}); \quad (4)$$

$$\frac{\partial F_{j,n}(v_{j,n}(t))}{\partial t} = \beta_1 (F_0 - F_{j,n}) + \beta_2 v_{j,n}, \quad \beta < 0, v_{j,n} > 0. \quad (5)$$

$$F(v_{j,n}) = -\infty \quad v_{j,n} \leq 0$$

where $j=1, \dots, N_x$ and $n=1, \dots, N_y$. N_x and N_y are the numbers of elements in the x - and y -directions. For general applicability to tribological problems Eq.(4) contains also a viscous term $\eta \partial u_j / \partial t$. Our calculations show that attractor properties are weakly influenced by the viscous term at sufficiently high velocities v_j . For generality, we keep small nonzero value $\eta=0.05$. Other parameters are: $\beta_1=1, \beta_2=125, F_0=1, k_1=1, k_2=36, v=0.2$.

Large scale structure of the wave state in the two-dimensional model with number of dimensionless grid cells ($N_x = 700, N_y = 300$) shown by the velocities $v=v(x,y;t) \equiv \partial u / \partial t$ is reproduced in Fig. 1 by the colored surface (MatLab color-map ‘jet’). Dark blue corresponds to zero. Mutual scattering manifests itself in high sharp peaks of the “events” reproduced here by the intensive red of the corresponding densities. Instant structure of the wave state and history of the events are combined in Fig. 2. The subplots (a) and (c) here represent snapshots of the instantaneous densities of the local displacements $u=u(x,y;t)$ and velocities $v=v(x,y;t) \equiv \partial u / \partial t$, respectively. Time-space representation of this process is shown in the subplot (b), and time dependency of total area of events (d). The information about attractor behavior is accumulated in Fig. 3 and briefly described in the caption to this figure.

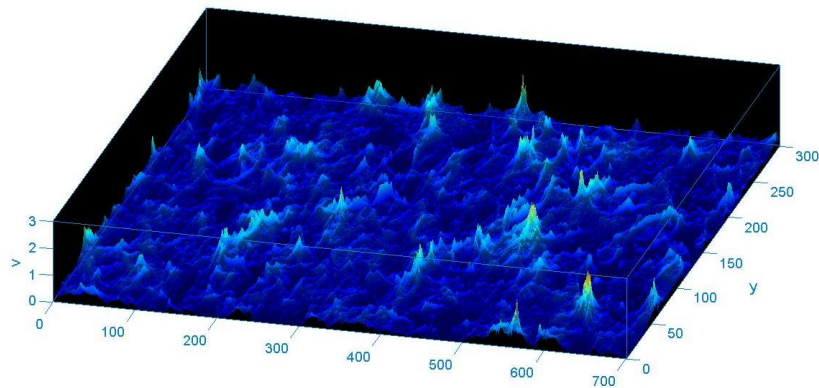


Fig. 1 Large scale structure of the wave state in the two-dimensional model shown by the velocities $v=v(x,y;t)\equiv\partial u/\partial t$ reproduced by the colored surface (MatLab color-map ‘jet’). Dark blue corresponds to zero. Mutual scattering manifests itself in high sharp peaks of the “events” reproduced here by the intensive red of the corresponding densities.

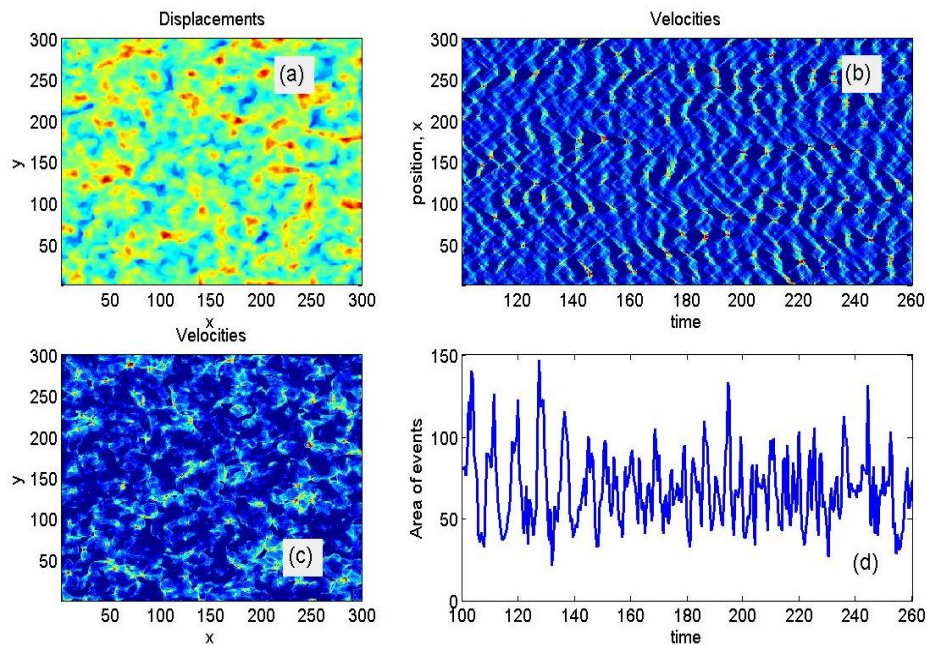


Fig. 2 Instant structure of the wave state and history of the events in the model. Subplots (a) and (c) represent snapshots of the instantaneous densities of the local displacements $u=u(x,y;t)$ and velocities $v=v(x,y;t)\equiv\partial u/\partial t$, respectively. The colormaps are equidistant and normalized to the intervals between maximum (red) and minimum (blue) values for the displacements $[-1,1]$ and velocities $[0, 1.5]$. Time-space representation of this process is shown in the (b) and (d) by the spatial-temporal map and time dependency of total area of events.

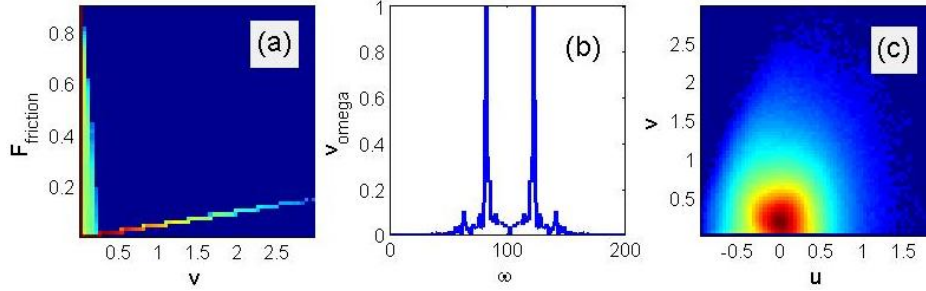


Fig. 3 The attractor of the variable effective friction in projection to the plane $\{v, F_{\text{friction}}\}$, where $\langle F_{\text{friction}} \rangle = \langle F[v_j(t)] + \eta v_j(t) \rangle$ is shown by color-map ‘jet’ in the subplot (a). The attractor behavior of the system causes quasi-periodic behavior of the mean area of the events. Correlation function in the subplot (b) here is calculated for the area of events shown in Fig. 2a. The same attractor is projected onto the plane $\{v, u\}$ in subplot (c).

To characterize the difference of the correlated and uncorrelated behavior, an order parameter has been introduced in ref. [25]. If we define a value h_j in block number j by the condition:

$$h_j = \begin{cases} 1 & \partial u_j / \partial t \neq 0 \text{ (the block is moving);} \\ 0 & \partial u_j / \partial t = 0 \end{cases}, \quad (6)$$

then the local density of the order parameter H_j^* can be written as $H_j^* = h_j(h_{j+1} + h_{j-1})$. This function takes on unit value $H_j^* = h_j(h_{j+1} + h_{j-1}) = 1$ if block j is moving and exactly one of its nearest neighbors is also moving. Further, $H_j^* = h_j(h_{j+1} + h_{j-1}) = 2$ when both nearest neighbors of the moving block are in motion. All other cases yield $H_j^* = 0$. Our observations with the modified model show that even for blocks at vanishing inter-block interaction $k_2 \rightarrow 0$ (when the motion of neighboring blocks is almost uncorrelated), the fraction of configurations where sets of neighboring blocks are moving is still relatively high. All that to say, the combination $H_j^* = h_j(h_{j+1} + h_{j-1})$ does not vanish in such an uncorrelated system. It is therefore convenient to construct another simple combination:

$$H_j = h_j h_{j+1} h_{j-1} = \begin{cases} 1 & \text{all 3 blocks } j, j+1, j-1 \text{ in contact are moving} \\ 0 & \text{otherwise} \end{cases}. \quad (7)$$

This makes $H_j = h_j h_{j+1} h_{j-1}$ zero in all cases except when both neighboring blocks of a central sliding block are also in motion. This combination can be used as an ‘‘order parameter’’. To extract integral quantitative information about the steady ordered and disordered states we calculate also the time evolution of the ensemble-averaged order parameter: $H(t) \equiv \langle H_j(t) \rangle = 1/t \int H_j(t) dt$.

As an illustration the dependence of the integrated order parameter on the stiffness k_2 , showing a transition from correlated to uncorrelated block motion was calculated for one-dimensional system. It is shown in Fig.4. Two well defined limiting cases can be seen easily: the order parameter tends to a constant non-zero asymptote $\langle H_j(t) \rangle \rightarrow \text{const} \neq 0$ at strong interaction $k_2 \gg 1$ and vanishes $\langle H_j(t) \rangle \rightarrow 0$ below the transition point $k_2 \approx 0$.

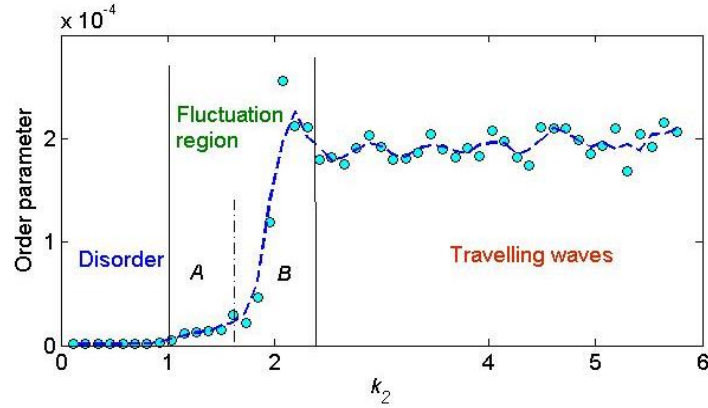


Fig. 4 Phase transition from correlated to uncorrelated motion of blocks in a one-dimensional system. The order parameter tends to a constant asymptote at high mutual interaction $k_2 \gg 1$ and vanishes below transition point $k_2 = k_{2,critical} \approx 1$. Two intermediate fluctuation regions A and B correspond to the states with short-range and long-range correlated nonlinear excitations, respectively.

Let us return now to general problem. If the interaction is already varied due to the motion with nonzero velocity, it sounds natural to modify the elasticity (potential channel of the interaction) of the system into the state dependent one, which varies at nonzero velocity and gradually returns to the initial one in static limit:

$$\frac{\partial k_2}{\partial t} = \alpha (k_{2;j+1,n} + k_{2;j-1,n} + k_{2;j,n+1} + k_{2;j,n-1} - 4k_{2;j,n}) + \lambda_1 (k_{20} - k_{k_{2;j,n}}) + \lambda_2 v_{j,n}. \quad (8)$$

The same note can be done about the thermalization of the system by a heating produced by the mechanical work performed by the external force. Local power consumed by the system in every node of the lattice can be calculated as a work per unit of time: $Q(r_{j,n}) = f_{j,n} v_{j,n}$. It can be treated as local source of energy acting in every node and temperature expansion inside the system should be described by the thermal conductivity equation:

$$\frac{\partial T_{j,n}}{\partial t} = \alpha (T_{j+1,n} + T_{j-1,n} + T_{j,n+1} + T_{j,n-1} - 4T_{j,n}) + Q(r_{j,n}). \quad (9)$$

It is possible to repeat all the simulations of the previous section, reproduce all the results presented in Figs.1-3 and demonstrate that these properties are common for all the modifications of the model. So, let us concentrate below on some additions coming from generalized version of the model.

Large scale structure of the velocity fluctuations analogous to that plotted in Fig. 1 accompanied by the variations of the elasticity self-consistently calculated according to Eq. (8) is shown by the colored surfaces (mainly red picks and blue smooth relief, respectively) in Fig. 5. One can see directly that strong fluctuations of the velocity cause deep valleys in the surface of elasticity and in turn “prefer” to appear in the same places again.

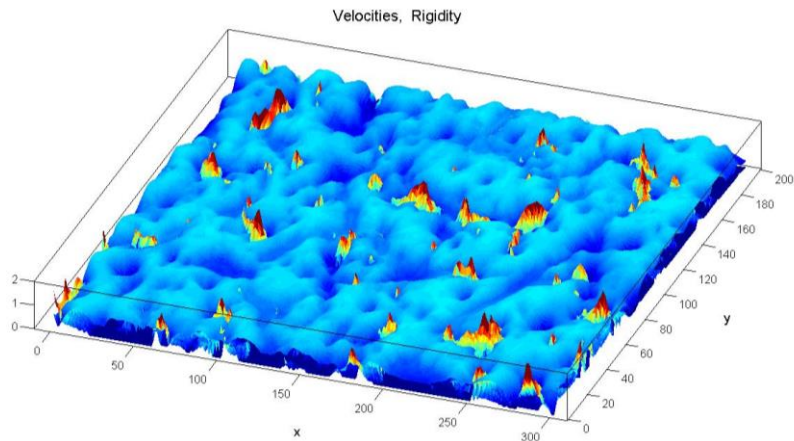


Fig. 5 Large scale structure of the velocity fluctuations accompanied self-consistently by the variations of the elasticity are shown by the colored surfaces (mainly red picks and blue smooth relief, respectively).

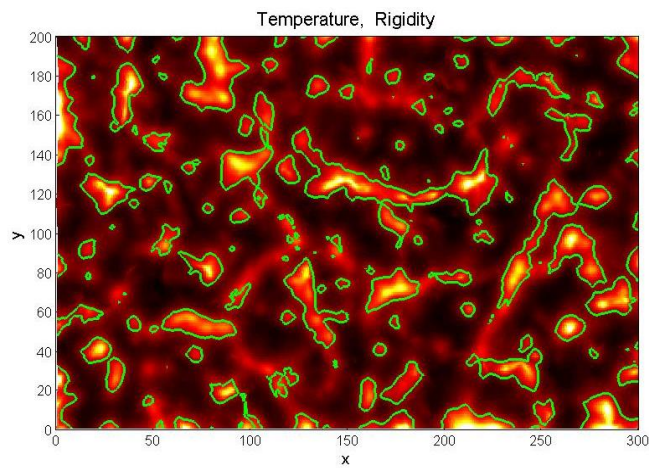


Fig. 6 The temperature deviations (bright spots in Matlab color-map 'hot' normalized in the interval $[0, 2]$) caused by the same instant configuration of the system as in Fig. 5. Green contour lines show median value of the elasticity profile and mark mutual correlation between its deep valleys and hot regions.

The same correlation exists between the spatially dependent elasticity and the temperature deviations. In Fig. 6 the temperature deviations (bright spots in Matlab color-map 'hot') caused by the same instant configuration of the system as in Fig. 5 are shown. Green contour lines show median value of the elasticity profile and mark mutual correlation between its deep valleys and hot regions.

To extract physically meaningful quantitative information about the earthquakes in the system different time moments one can calculate a density of power consumed by the

system at each time moment and overlap it other densities of the system like: distributed rigidity, friction constant and temperature. The local power in the frames of the model can be calculated as a work produced by the forces acting on each lattice node of the system $p_{ij} = \mathbf{f}_{ij} \mathbf{v}_{ij}$ during a unit of time. Calculating spatially distributed power $p_i = \mathbf{f}_i \mathbf{v}_i$ enables one to evaluate the degree of localization of excitations and hence the fraction of the regions in which the fragments of the lattice move practically as a whole. As at a particular site the energy is absorbed and released at different points in time, it is useful to characterize these sites by the absolute value of the power, $|p_i| = |\mathbf{f}_i \mathbf{v}_i|$. However, if formally accumulate the statistics of such “events” using all the nodes as independent realizations, strongly overestimated value of the small “events” will be obtained. Physically only the quakes with a magnitude higher than a critical one would be treated as the observable ones. Moreover, if the amplitude of the power exceeds the critical value for a number of mutually connected nodes, all of them will be treated by the potential observers as one common event with an average amplitude in this connected area. So, we organized the procedure in this manner: all the nodes were found with the amplitudes higher than the critical one; defined all the connected domains of them and calculated mean amplitudes for every such a region. To control visually the above procedure, we plotted these domains by the (bright) ‘jet’ colors over the (blue) map of the rigidity for every time moment. Typical instant realization of such a picture is presented in Fig. 7. The histogram calculated for these events, as it is shown in Fig. 8 in double-logarithmic scale.

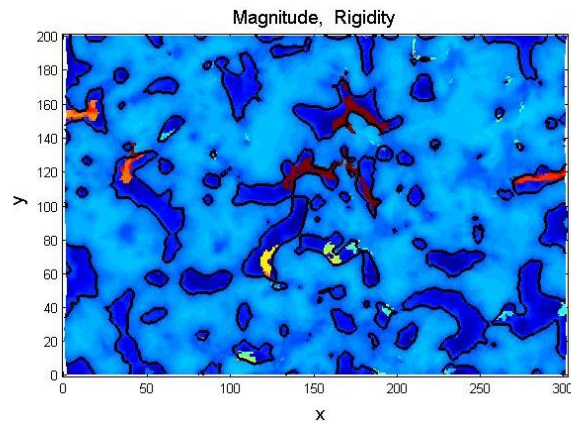


Fig. 7 Instant connected regions of the “earthquakes” (bright spots) and valleys of the small rigidity (deep blue) plotted together to illustrate their mutual correlations. The artificial colors for the magnitude and rigidity are shifted to red and blue parts of the spectrum to clearly overlap both densities in one picture.

As we already noted above the variations of the friction, elasticity and local velocities are mutually correlated. In other words, new events are preferably generated in the same regions (as it is in the reality). As a result, the system partially memorizes such a common relief for extremely long times. One can calculate, for example, time-averaged relief of effective rigidity, and we did this. It is quite expected that the variations are found to be much smaller than local instant variations of the same value, but they exist.

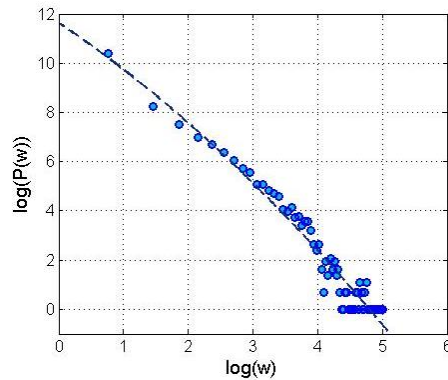


Fig. 8 Scaling of the probability to find an earthquake with a particular value of magnitude calculated for the connected event regions. Physically it corresponds to a selection of the rare but intensive “events”, which is compatible with the ideology of the empirical Gutenberg-Richter law.

There are also some correlations between such a memorized structure and preferable channels of the wave propagation. Again, the correlation is much weaker than it is observed between instant variations of different densities, but it still exists. These results are illustrated in Fig. 9, where instant and almost stationary time averaged elastic coefficient integrated over long time periods ((a) and (b) sub-plots, respectively) shown by the ‘jet’ color-map. Black contour line depicts mean value of the long-time living rigidity surface. It marks only partial correlations between the averaged and instant rigidities, Analogous (only partial) correlation is found between travelling regions of maximal power production (deep red spots in subplot (b)) and time-averaged relief of the rigidity.

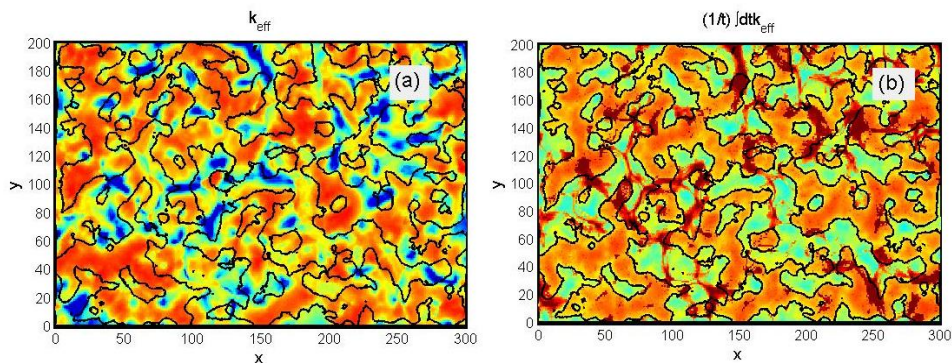


Fig. 9 Instant and almost stationary time averaged elastic coefficient integrated over long time periods ((a) and (b) subplots, respectively) shown by the ‘jet’ color-map. Contour line marks only partial correlations between the averaged and instant rigidities, Analogous (only partial) correlation is found between travelling regions of maximal power production (deep red spots in subplot (b)) and time-averaged relief of the rigidity.

3. MOVABLE AUTOMATA MODEL

Generally, the variant of the model which uses movable system is based on a description of a system of interacting N “particles”. In contrast to described above lattice model which treats system as deformable elastic medium with varied friction and rigidity, here each “particle” simulates a complete block (“solid plate”) in some instant position represented radius-vector \mathbf{r}_i of its center and the mechanical momentum \mathbf{p}_i . In simplest approximation, the plates interact with a potential $U(\mathbf{r}_i - \mathbf{r}_j)$ depending on the distance $|\mathbf{r}_i - \mathbf{r}_j|$ between their centers. It formally leads to the following many-body Hamiltonian:

$$H(\mathbf{r}_i, \mathbf{p}_i) = \sum_{i=1}^N \mathbf{p}_i^2 / 2m_i + \sum_{i,j=1}^N U(|\mathbf{r}_i - \mathbf{r}_j|) / 2. \quad (10)$$

In a static configuration the plates are supposed to occupy some equilibrium positions defined by a competition of the repulsion and attraction forces acting between them. In the context of this study, it is convenient to represent the interaction potential by a pair of the Gauss potentials:

$$U(|\mathbf{r}_i - \mathbf{r}_j|) = C_{ij} \exp\{-[(\mathbf{r}_i - \mathbf{r}_j) / c_{ij}]^2\} - D_{ij} \exp\{-[(\mathbf{r}_i - \mathbf{r}_j) / d_{ij}]^2\}, \quad (11)$$

where C_{ij} and D_{ij} define the magnitude, while c_{ij} and d_{ij} the radii of attraction and repulsion, respectively. The minimization of the energy corresponding to a desired equilibrium with some characteristic distance between the centers corresponds to the inequalities between the parameters: $C_{ij} \gg D_{ij}$, $c_{ij} < d_{ij}$. Initially, correct equilibrium positions of the plates are not known and should be found by a self-assembling transient process. To obtain it in numerical experiments, the “particles” are initially placed at random on a rectangle with the side lengths of $[0, L_x]$ and $[0, L_y]$. During the transient process the system finds some frozen structure which is a compromise between the interactions and boundary conditions.

Depending on the particular study, the boundary conditions can be chosen differently. For example, for the case of shear deformation, it is convenient to employ periodic boundary conditions on the horizontal axis. It allows simulate potentially infinite run for relatively small limited numerical arrays. According to the periodic boundary conditions, a particle leaving the interval $[0, L_x]$ is returned to it at the opposite end and the vectors $\mathbf{r}_i - \mathbf{r}_j$ connecting particles either located within the interval $[0, L_x]$ or the images of “escaped” particles at the opposite side of the system. On the vertical axis such a system can be limited by the horizontal plates at $y=0$ and $y=L_y$ with reflecting boundary conditions: $U_{up} = C \cdot \exp[(y - L_y)/c]$ and $U_{down} = C \cdot \exp[-y/c]$. Such a combination of the boundary conditions simulates together quasi-infinite motion along horizontal axis and confined motion between two “external” plates in orthogonal direction. The stronger the inequalities $C \gg C_{ij}$ and $c \ll c_{ij}$, the more rigid and sharp are the walls in relation to other forces and lengths relevant to the system.

Keeping in mind typical “tectonic” geometry with the moving continents, in the present study we are interested in a configuration when along horizontal axis the system is also limited and moreover, is pressed by a movable “rigid wall”. In analogy with standard Burridge-Knopoff model, the plate is driven by an external “elastic” force:

$$F_{ext} = K(L_x - V_0 t), \quad (12)$$

In this case it is natural, in contrast to the periodic one, to take the system which is limited along horizontal axis with reflecting boundary conditions: $U_{right}=C \cdot \exp[(x-L_x)/c]$ and $U_{left}=C \cdot \exp[-x/c]$, but with the movable right boundary $L_x=L_x(t)$.

Since the parameters C_{ij} , D_{ij} , c_{ij} and d_{ij} form arrays covering all possible combinations, it can be said without loss of generality that the Hamiltonian given by Eqs. (10)- (12) describes systems with any number of components (plates of the different sizes). What is required is just to specify the parameters C_{jk} and c_{jk} . In a real system different values of all the parameters (and what is even more important, the mutual relations between them) regulate different sizes of the physical plates and their mutual rigidity. Below, to conserve a generality and get statistically representative results, we use the values C_{jk} , and c_{jk} randomly varied with 10 times difference between maximal and minimal ones around unit C_{jk} , $c_{jk}=1$, and reset them from one run to another of every numerical experiment performed at other fixed or systematically varied parameters.

The simplicity of the equations of motion

$$m_i \partial \mathbf{v}_i / \partial t = -\partial H(\mathbf{x}_i, \mathbf{p}_i) / \partial \mathbf{p}_i = \mathbf{f}_i, \quad (13)$$

is deceptive. In majority of the cases, simulation using such equations is extremely time-consuming because it involves a summation at every time step over all possible neighbors, including very distant ones (and even fictitious image particles in the case of periodic boundary conditions). However, in the case of the solid plates contacting by their boundaries the number of the mutual interactions can be essentially reduced. The reduction is based on the following considerations.

It is natural for this particular problem to construct Voronoi diagram of the set of effective “particles” and associate each cell of this diagram with some of the mutually contacting plates. According to mathematical definition, a Voronoi diagram is a partition of a plane into regions close to each of a given set of objects. In the simplest case, these objects are just set of points in the plane (called seeds). For each seed there is a corresponding region, called a Voronoi cell, consisting of all points of the plane closer to that seed than to any other. In our case the central “particles” of every “plate” play a role of such mathematical “seeds”.

So, the cells of Voronoi diagram give practically the same picture, which we have in mind when building our dynamic model. Every such a cell is surrounded by the limited (and in fact quite small) number of the other plates (nearest neighbors). Mathematically such neighbors are completely defined by the Delaunay triangulation, which is dual to the Voronoi diagram. According to its definition, Delaunay triangulation for a given set P of discrete points in a general position is a triangulation DT(P) such that no point in P is inside the circumcircle of any triangle in DT(P). As result one gets quite realistic representation of the movable plates and short list of the neighbors interacting with every particular plate.

Interacting plates exchange momentum, and hence a dissipation channel acting to equilibrate the relative velocities of particles (that happen to be within the distance c_v , close to the equilibrium one) needs to be introduced. This can be done by including an additive velocity-depending force.

$$\mathbf{f}_i^v = \eta \sum_{j=1}^{N_{neighbours}} (\mathbf{v}_i - \mathbf{v}_j) \exp\left[-[(\mathbf{r}_i - \mathbf{r}_j) / c_v]^2\right], \quad (14)$$

acting on the i -th particle, with some dissipation constant η . As a result, the equations of motion assume the following form:

$$m_i \frac{\partial v_i}{\partial t} = f_i^r - f_i^v. \quad (15)$$

They can be integrated by using Verlet's method, which conserves the energy of the system at each time step, provided no energy is supplied externally through mechanical work of the movable right boundary which is driven by a balance of the external force $F_{ext}=K(L_x-V_0t)$ and total interaction with the internal plates repulsed by the boundary potential $U_{right}=C \cdot \exp[(x-L_x)/c]$

$$M \frac{\partial^2 L_x}{\partial t^2} = F_{ext} - \sum_{j=1}^N \partial U_{right}(x_j - L_x(t)) / \partial x_j. \quad (16)$$

So, the equations (15) and (16) must be solved self-consistently. Moreover, counting on the nature of the problem under consideration, this system has to be accompanied by the equations regulating variation of the effective mutual friction between the plates with negative derivative in the same spirit as it was done above for the standard BK model on the elastic lattice:

$$\frac{\partial F_j}{\partial t} = \beta_1 (F_0 - F_j(v_j, t)) + \beta_2 v_j; \quad \beta_2 < 0, \quad v_{j,n} > 0 \quad \text{and} \quad F(v_j) = -\infty \quad \text{at} \quad v_j < 0. \quad (17)$$

Taking into account an experience which obtained in modification lattice BK model it seems natural to add here also variable intensity of the interactions between the plates at nonzero mutual velocities:

$$\frac{\partial C_{1j}}{\partial t} = \lambda_1 (C_{10} - C_{1j}(v_j, t)) + \lambda_2 v_j; \quad \lambda_2 < 0, \quad v_{j,n} > 0 \quad \text{and} \quad C_1(v_j) = C_{10} \quad \text{at} \quad v_j < 0. \quad (18)$$

At the same time, here is no need to include directly the temperature conductivity equation into the model because it is already based on the Brownian dynamic equations for the plate centres by itself, and in fact automatically involves an exchange by kinetic energy (temperature) between them. So, plotting the kinetic energy of the "particles" by the artificial colors one gets a color-map in the representation which is natural for the model based on the movable automata. The results obtained in the frames of this model are summarized in the Figs. 10-15 below.

Typical instant configuration of the plates pressed from one of the boundaries by an external force is shown in Fig. 10. Let us remind that the rigid wall presses the system from the right side. As a result, it becomes more compressed from this side and areas of the Voronoi cells here become smaller than in average inside the system far from this boundary. The mass of every plate conserves in the frame of the model. The only are of it changes. Gray-scale map of the subplot (a) is used to show the individual areas of the plates.

The compression and motion of the plates causes nonzero mutual velocities of every plate in relation to their proximities. This fact is well seen in the subplot (b) by the MatLab 'jet' color-map. According to Eq.(17) nonzero mutual velocities result in a variation of the effective friction between every plate and its surrounding. This characteristic of the system is depicted in the subplot (c). It is important to note also that the Delaunay triangulation is recalculated at every time step. As a result, the links between the plates moving with different velocities can appear and disappear depending on their physical positions at a particular time moment. However, in sufficiently dense

system (which is used here) such changes of the neighbors happen quite rarely. So, the model seems quite realistic to describe some features of the tectonic motion.

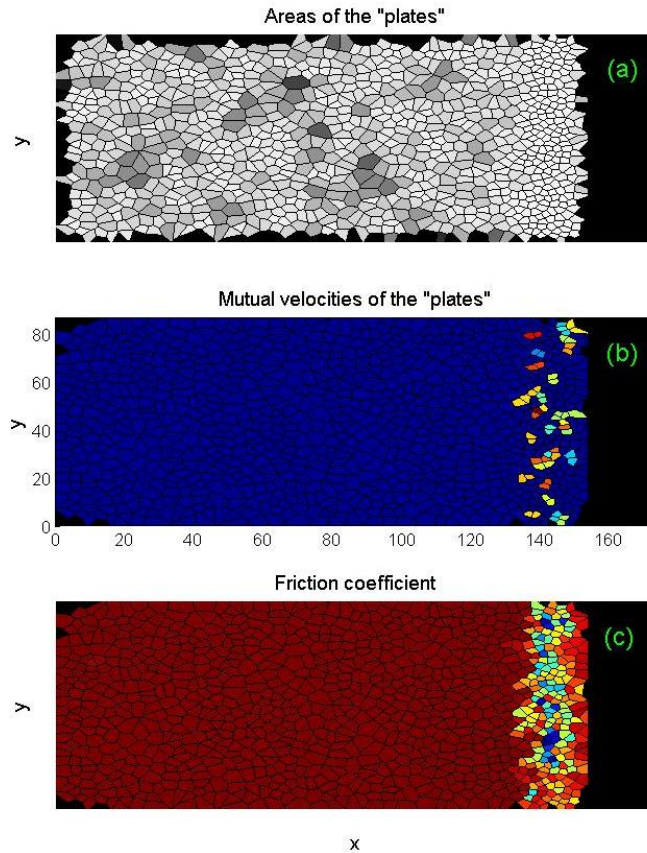


Fig. 10 Typical instant configuration of the plates pressed from one of the boundaries by an external force. Gray-scale map of the subplot (a) shows the areas of the plates more compressed from one side (white color) than inside the system (different intensity of gray color). The compression and motion of the plates causes different (mean) mutual velocity of every plate in relation to its proximity which results in the variation of the effective friction between this plate and surrounding ones. Both these characteristics are plotted by the ‘jet’ colors.

Fine structure of the model is presented in Fig. 11. Movable Voronoi diagram in subplot (a) here show the plates in the frame of the model, as above. However, here they are accompanied by the colored seeds of the Voronoi cells. The colors show different instant velocities of the plates. Dual to the above diagram Delaunay triangulation shows connections between the plates and their neighbors counted in the model. According to its mathematical definition it naturally gives a list of the neighbors for every plate. So, one can calculate the interactions between them, solve the dynamic equations, so on. Different

sizes of the nodes here reproduce different (randomly distributed) interaction parameters. Besides, it is convenient to control instant number of them for every cell (symmetry of the plate polygon) and visualize it by the colors from the same standard 'jet' map.

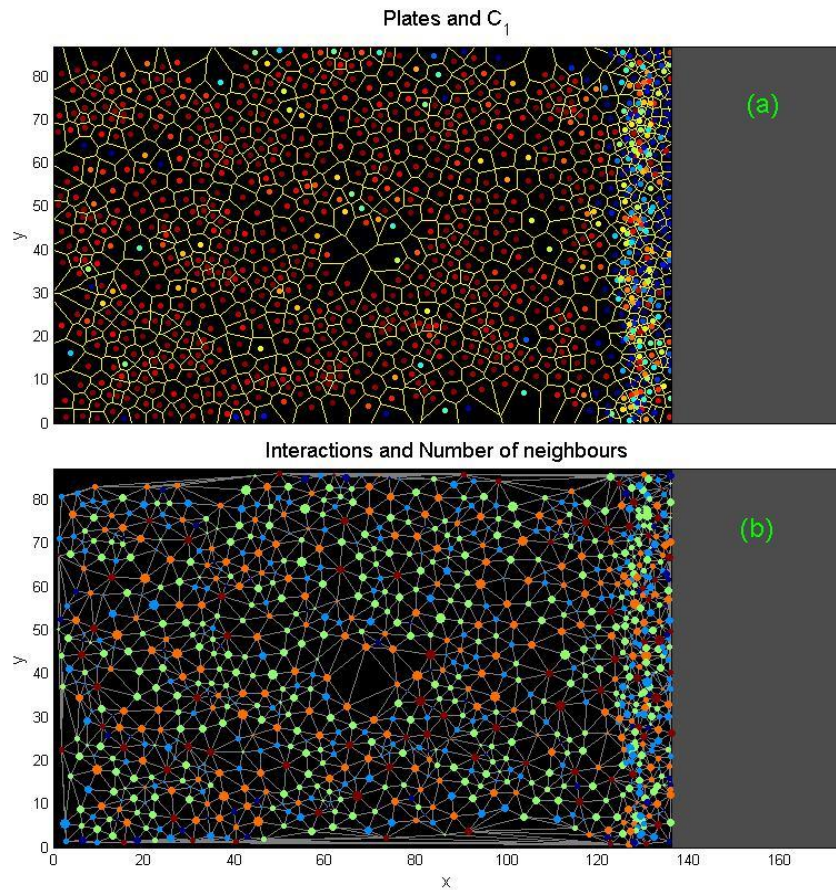


Fig. 11 Movable Voronoi diagram in subplot (a) describes the plates in the frame of the model. The colors of the seeds show different instant velocities of the plates. Dual to the above diagram Delaunay triangulation shows connections between the plates and their neighbors counted in the model. Different sizes of the nodes here reproduce different interaction coefficients and their colors show different instant number of neighbors.

Two projections of the phase portrait on different planes (subplots (a) and (b)) are presented in the Fig. 13 by the colored circles of different sizes. The colors and sizes of the circles have the same meaning as in the Fig. 12a. Green line with the arrows shows typical individual trajectory, which every point passes through the phase space with the time and reproduces the evolution of the effective friction due to periods of large or small

local velocities. Generally, the subplot (b) here has the same physical meaning as the phase portrait plotted in Fig. 3a in the lattice variant of BK model.

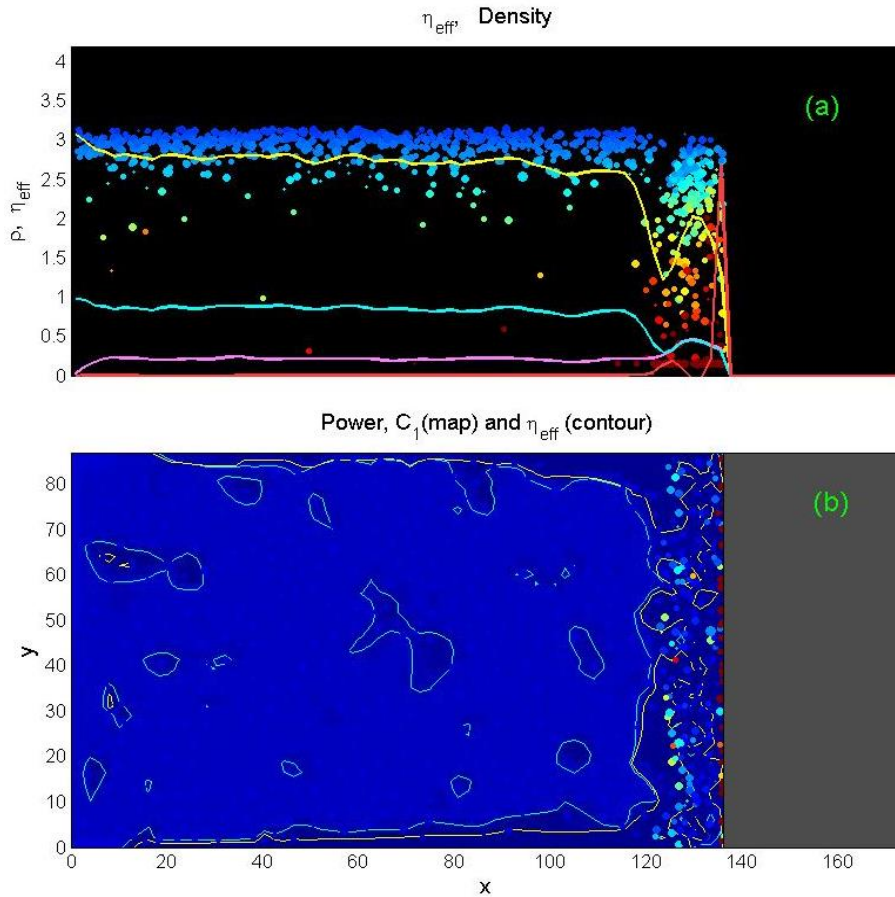


Fig. 12 The same instant configuration as in Fig. 11 reproducing mutual relations between the interactions, local rigidities, velocities and friction coefficient directly marked in the plots. The colors and sizes of the individual circles in the subplot (a) depict velocities and interaction coefficients of the individual plates, respectively. Yellow, cyan, magenta and red lines in the subplot (a) display integrated over y -coordinate averaged x -dependencies of the velocity, rigidity, effective friction coefficient density and temperature respectively. The colors of the circles in the subplot (b) correspond to different individual power of the events in every plate.

To get the local power in the frames of the discrete variant of the model we calculate the work produced by the forces acting on each plate (seed) of the system $p_i = \mathbf{f}_i \mathbf{v}_i$. Calculation of spatially distributed power $p_i = \mathbf{f}_i \mathbf{v}_i$ enables one to evaluate the degree of localization of excitations and hence the fraction of the regions in which the fragments of the lattice move practically as a whole. As at a particular site the energy is absorbed and

released at different points in time, it is useful to characterize these sites by the absolute value of the power, $|p_i|=|\mathbf{f}_i\mathbf{v}_i|$. It is shown in subplot (b) of the Fig.12.

Summation over all particles yields the total power $VF_{ext}(t)=P(t)=\sum\mathbf{f}_i\mathbf{v}_i$. It gives an energy which is consumed during every time unit due to motion of rigid right boundary, which is forced by external flow with constant velocity, $V=const$. However, the boundary here is moving with some varied velocity $V(t)$ which is determined by a balance of the total force, $F_{ext}(t)$ and only its time average coincides with $\langle V(t)\rangle=V_0$.

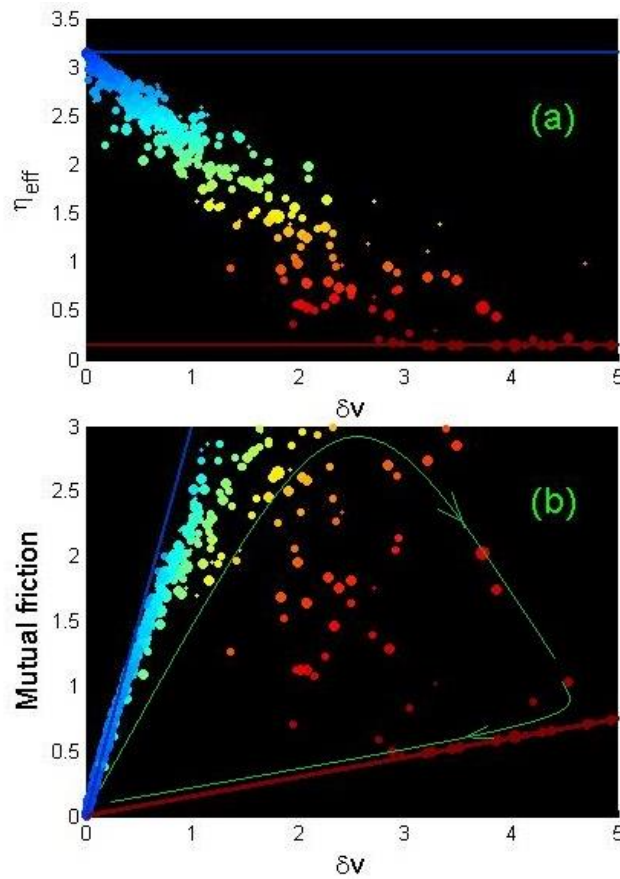


Fig. 13 Two projections of the phase portrait on different planes (subplots (a) and (b)). The colors and sizes of the circles depict velocities and interaction coefficients of the individual plates, respectively. Green line with the arrows shows typical individual trajectory, which every point passes in phase space with the time.

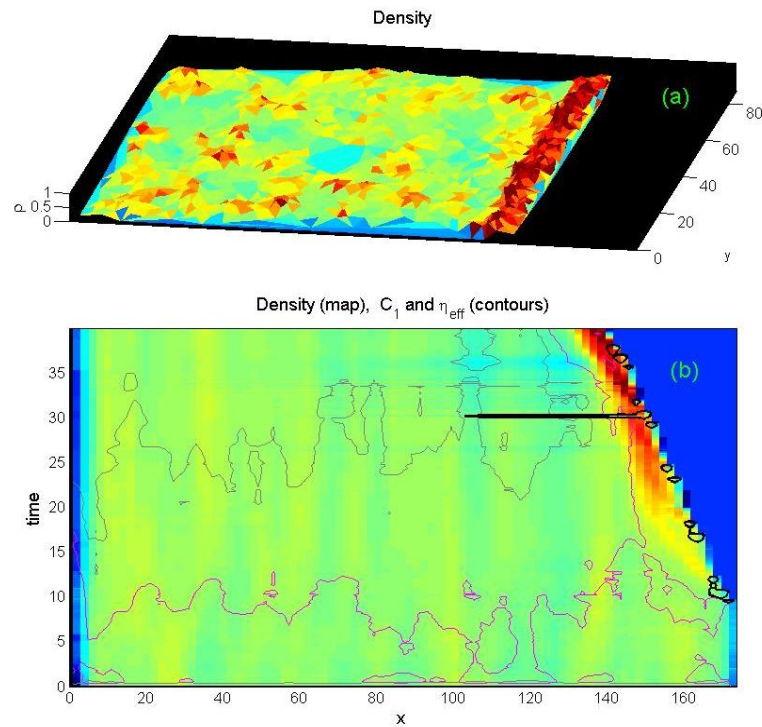


Fig. 14 Instant configuration of the density (surface in subplot (a)) and time-space diagram of the history of events (colormap in subplot (b)). Bold black contours mark intensive “earthquake” events near the propagating right boundary. Different speed of the front and some “epochs” of intensive events can be seen from different inclination of the front and horizontal lines in the recorded history.

In particular, it causes quasi-periodic oscillations of the velocity of boundary which are typical for the “stick-slip” nature of the processes. It is actually the same phenomenon, which takes place in ordinary BK model, shown above in Figs. 2-3. In the discrete model one can additionally observe the waves of the velocities, densities and power of the events, which are accompanied by quasi-periodic “epochs” of intensive “earthquakes”.

Instant configuration of the density and history of the density integrated along y -axis corresponding to the magenta curve in Fig. 12a are shown in Fig. 14. The instant surface is plotted in subplot (a) and corresponding time-space diagram of the history of events is presented in the subplot (b). Bold black contours mark intensive “earthquake” events near the propagating right boundary. Different speed of the front and some “epochs” of intensive events can be seen from different inclination of the front and deeply colored almost horizontal lines in the recorded history.

Exactly the same history of the events (recorded during the same calculation run) as in Fig. 14, is depicted by the intensity of power production (shown by the ‘hot’ color map). The epochs of the intensive earthquakes are much stronger pronounced here than in the previous figure.

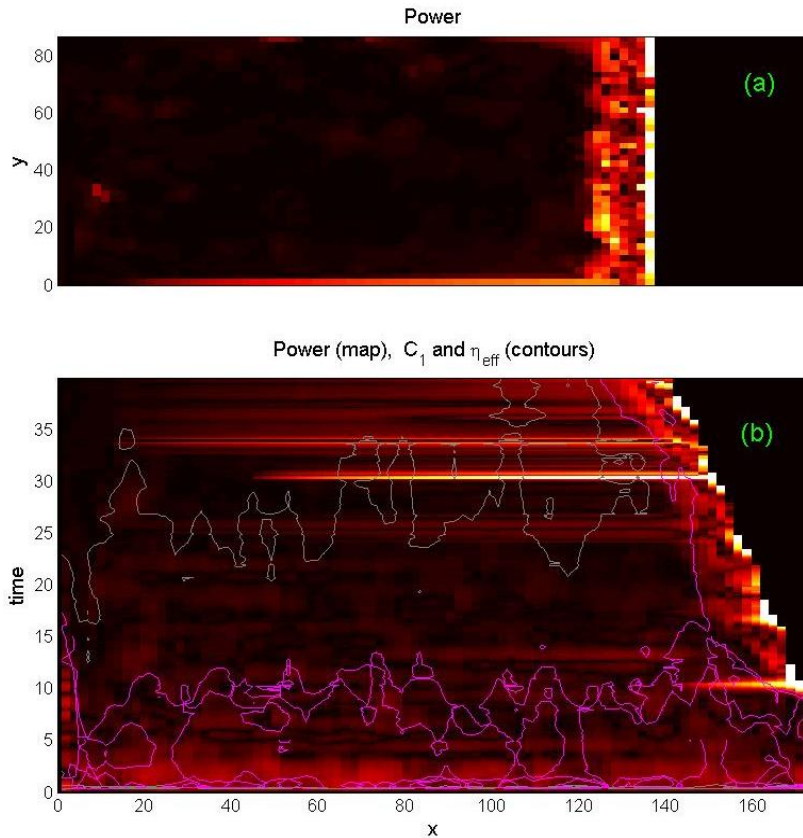


Fig. 15 Exactly the same history of the events, as in Fig.14, depicted by the intensity of power production (shown by the 'hot' colormap). The epochs of the intensive earthquakes are much stronger pronounced here than in the previous figure.

4. CONCLUSION

It is shown that original Burridge-Knopoff model allows a number of the modifications which can increase its ability to be adapted to description of the different practically important features of the tectonic phenomena. Basic modifications of the model were already made previously. They incorporate naturally introduced state dependent friction where the friction force is defined by the additional kinetic equation as well as extension of the model to more realistic two-dimensional case.

In the present paper we continued previous modifications and mainly concentrated on the following extensions of the model. First of all, elastic force and thermal conductivity were added into consideration. Besides to the velocity weakening of friction between moving blocks, we combined an increase of both static friction and rigidity during stick periods as well their simultaneous weakening during motion. It is expected to give better and qualitatively correct description of plural transitions from smooth sliding to stick-slip

behavior, which are normally observed in various tribological and tectonic systems. To get easier comparison with the previous versions of the model we initially did this using in standard approach based on interacting elastically connected mesh elements.

An alternative version of the model is finally proposed. It applies a simulation of the motion of relatively large solid blocks, utilizing technique of the movable cellular automata. In this advanced version we also involve all the components of the real system: state depending friction, changeable rigidity, as well as heat production and thermal conductivity due to dynamics of the interacting plates, which were already included into the previous versions based on traditional lattice model.

Proposed modification has its own advantages and disadvantages, which were discussed in the paper step by step. However, a combination of the different approaches gives additional degrees of freedom, which allows select more convenient or adequate approach depending on the particular problem under consideration. We plan to continue further and combine our studies in both alternative directions.

REFERENCES

1. Gutenberg, B., Richter, C.F., 1994, *Frequency of earthquakes in California*, Bulletin of the Seismological Society of America, 34(4), pp. 185-188.
2. Bak, P., Christensen, K., Danon, L., Scanlon, T., 2002, *Unified scaling law for earthquakes*, Physical Review Letters, 88, 178501.
3. Žalohar, J., *Omori's Law*, 2018, Chapter 10 in the book "Developments in Structural Geology and Tectonics", Elsevier, pp. 123-134.
4. Bak, P., Tang, C., Wiesenfeld, K., 1987, *Self-organized criticality: An explanation of the 1/f noise*, Physical Review Letters, 59, 381.
5. Carlson, J.M., Langer, J.S., 1989, *Properties of earthquakes generated by fault dynamics*, Physical Review Letters, 62, 2632.
6. Ruzhich, V.V., Smekalin, O.P., Shilko, E.V., Psakhie, S.G., 2002, *About nature of "slow waves" and initiation of displacements at fault regions*, In: Proceedings of the international conference on new challenges in mesomechanics, pp.311-318.
7. Ruzhich, V.V., Truskov, V.A., Chernykh, E.N., Smekalin, O.P., 1999, *Neotectonic movements in fault zones of the Baikal region and their origin mechanisms*, Russian Geology and Geophysics, 40(3), pp. 356-368.
8. Psakhie, S.G., Shilko, E.V., Astafurov, S.V., 2004, *Peculiarities of the mechanical response of heterogeneous materials with highly deformable interfaces*, Technical Physics Letters, 30, pp. 237-239.
9. Psakhie, S.G., Ruzhich, V.V., Shilko, E.V., Popov, V.L., Dimaki, A.V., Astafurov, S.V., Lopatin, V.V., 2005, *Influence of the state of the inter-block interfaces on the character of local displacements in block-structured media*, Technical Physics Letters, 31, pp. 712-715.
10. Ruzhich, V.V., Psakhie, S.G., Bomyakov, S.A., Smekalin, O.P., Shilko, E.V., Chernykh, E.N., Chechelnitzsky, V.V., Astafurov, S.V., 2002, *Investigation of influence of vibroimpulse excitations on regime of displacements in seismically active fault regions*, Phys. Mesomech., 5(5), pp. 85-96.
11. Bhattacharya, P., Chakrabarti, B.K., Samanta, K.D., 2009, *Fractal models of earthquake dynamics*, Heinz Georg Schuster (ed), *Reviews of Nonlinear Dynamics and Complexity*, Wiley-VCH, pp. 107-150.
12. Ford, J., 1992, *The Fermi-Pasta-Ulam problem: Paradox turns discovery*, Physics Reports, 213(5), pp. 271-310.
13. Lichtenberg, A.J., Lieberman, M.A., 1992, *Regular and Chaotic Dynamics*, Springer, New York, 692 p.
14. Filippov, A.E., Hu, B., Li, B., Zeltser, A., 1998, *Energy transport between two attractors connected by a Fermi-Pasta-Ulam chains*, Journal of Physics A: Mathematical and General, 31, 7719.
15. Filippov, A.E., Popov, V.L., Psakhie, S.G., 2006, *Converting displacement dynamics into creep in block media*, Technical Physics Letters, 32(6), pp. 545-549.
16. Filippov, A.E., Popov, V.L., Psakhie, S.G., 2008, *Correlated impacts optimizing the transformation of block me-dium dynamics into creep regime*, Technical Physics Letters, 34(8), pp. 689-692.

17. Filippov, A.E., Popov V.L. 2021, *Study of Dynamics of Block-Media in the Framework of Minimalistic Numerical Models*, Chapter 7 in the book «Multiscale Biomechanics and Tribology of Inorganic and Organic Systems», Springer International Publishing, pp. 143-168.
18. Burridge. R., Knopoff, L., 1967, *Model and Theoretical Seismicity*, Bulletin of the Seismological Society of America, 57(3), pp. 341-371.
19. Bruce, S.E., Carlson, J.M., Langer, J.S., 1992, *Patterns of seismic activity preceding large earthquakes*, Journal of Geophysical Research, 97, pp. 479-488.
20. Carlson, J.M., Langer, J.S., Shaw, B.E., 1994, *Dynamics of earthquake faults*, Review of Modern Physics, 66(2), pp. 657-670.
21. Saito, T., Matsukawa, H., 2007, *Size dependence of the Burridge-Knopoff model*, Journal of Physics: Conference Series, 89, 012016.
22. Mandelbrot, B., 1982, *The Fractal Geometry of Nature*, Freeman and Co., San Francisco, 460 p.
23. Pelletier, J.D., 2000, *Spring-block models of seismicity: review and analysis of a structurally heterogeneous model coupled to the viscous asthenosphere. Geocomplexity and the Physics of Earthquakes*, Geophysical Monographs, American Geophysical Union, pp.27-42.
24. Muratov, C.B., 1999, *Traveling wave solutions in the Burridge-Knopoff model*, Physical Review E, 59, 3847.
25. Huisman, B.A.H., Fasolino, A., 2005, *Transition to strictly solitary motion in the Burridge-Knopoff model of multicontact friction*, Physical Review E, 72, 016107.
26. Clancy, I., Corcoran, D., 2005, *Criticality in the Burridge-Knopoff model*, Physical Review E, 71, 046124.
27. Clancy, I., Corcoran, D., 2006, *Burridge-Knopoff model: Exploration of dynamic phases*, Physical Review E, 73, 046115.
28. Mori, T., Kawamura, H., 2008, *Simulation study of earthquakes based on the two-dimensional Burridge-Knopoff model with long-range interactions*, Physical Review E 77, 051123.
29. Dieterich, J.H., 1974, *Earthquake mechanisms and modeling*, Annual Review of Earth and Planetary Sciences, 2, pp. 275-301.
30. Dieterich, J.H., 1978, *Time-dependent friction and the mechanics of stick-slip*, Pure and applied geophysics, 116, pp. 790-806.
31. Rice, J.R., Gu, J.C., 1983, *Earthquake aftereffects and triggered seismic phenomena*, Pure and applied geophysics, 121, pp. 187-219.
32. Gu, J.C., Rice, J.R., Ruina, A.L., Tse, S.T., 1984, *Slip motion and stability of a single degree of freedom elastic system with rate and state dependent friction*, Journal of the Mechanics and Physics of Solids, 32(3), pp. 167-196.
33. Marone, C., 1998, *Laboratory-derived friction laws and their application to seismic faulting*, Annual Review of Earth and Planetary Sciences, 26, pp. 643-696.
34. Persson, B.N.J., 2000, *Sliding Friction, Physical Properties and Applications*, Springer, Berlin.
35. Popov, V.L., 2010, *Contact Mechanics and Friction Physics*, Springer, Berlin, 362p.
36. Popov, V.L., 2000, *A theory of the transition from static to kinetic friction in boundary lubrication layers*, Solid State Communications, 115(7), pp. 369-373.
37. Filippov, A.E., Klafter, J., Urbakh, M., 2004, *Friction through dynamical formation and rupture of molecular bonds*, Physical Review Letters, 92, 135503.
38. Fermi, E., Pasta, J., Ulam, S., Tsingou, M., 1993, *The Many-body Problem: An Encyclopedia of Exactly Solved Models in One Dimension*, World Scientific, Singapore, 988 p.
39. Braun, O.M., Hu, B., Filippov, A.E., Zeltser, A., 1998, *Traffic jams and hysteresis in driven one-dimensional systems*, Physical Review E, 58, 1311.
40. Filippov, A.E., 1994, *Mimicry of phase transitions and the large-river effect*, JETP Lett., 60(2), pp. 133-137.
41. Filippov, A.E., Popov, V.L., 2010, *Modified Burridge-Knopoff model with state dependent friction*, Tribology International, 43, pp. 1392-1399.
42. Ohmura, A., Kawamura, H., 2007, *Rate-and state-dependent friction law and statistical properties of earthquakes*, Europhysics Letters, 77, 69001.
43. Persson, B.N.J., Popov, V.L., 2000, *On the origin of the transition from slip to stick*, Solid State Communications, 114(5), pp. 261-266.
44. Balokhonov, R., Romanova, V., Zemlianov, A., 2021, *A mesoscopic analysis of a localized shear band propagation effect on the deformation and fracture of coated materials*, Reports in Mechanical Engineering, 2(1), pp. 6-22.
45. Romanova, V., Balokhonov, R., Zinovieva, O., 2021, *Mesoscale deformation-induced surface phenomena in loaded polycrystals*, Facta Universitatis-Series Mechanical Engineering, 19(2), pp. 187-198.
46. Kocharyan, G.G., Kishkina, S.B., 2021, *The Physical Mesomechanics of the Earthquake Source*, Phys. Mesomech., 24, pp. 343–356.

47. Makarov, P.V., Khon, Y.A. Autosoliton View of the Seismic Process. 2021, *Part 1. Possibility of Generation and Propagation of Slow Deformation Autosoliton Disturbances in Geomedia*, Phys. Mesomech., 24, pp. 363–374.
48. Makarov, P.V., Smolin, I.Y., Khon, Y.A., et al. 2021, *Autosoliton View of the Seismic Process. Part 2. Possibility of Generation and Propagation of Slow Deformation Autosoliton Disturbances in Geomedia*, Phys. Mesomech., 24, pp. 375–390.